Journal of Solid Mechanics Vol. 13, No. 2 (2021) pp. 144-163
DOI: 10.22034/jsm.2020.1891091.1539

Linear and Nonlinear Free Vibration of a Two-Dimensional Multiferroic Composite Plate Subjected to Magneto-Electro-Thermo-Aerodynamic Loading

S. Razavi [1,*], H. Ghashochi-Bargh [2]

[1]*Department of Mechanical Engineering, Tabriz Technical and Vocational College, Tabriz, Iran*
[2]*Imam Khomeini International University- Buein Zahra, Higher Education Center of Engineering and Technology, Qazvin, Iran*

Received 17 February 2021; accepted 4 April 2021

ABSTRACT

Vibration response of a two-dimensional magneto-electro-elastic plate is investigated in this paper. The considered multi-phase plate is rectangular and simply-supported resting on an elastic foundation. The plate is under aerodynamic pressure and subjected to temperature change. It is also assumed that the magneto-electro-elastic body is poled along the z direction and subjected to electric and magnetic potentials between the upper and lower surfaces. The nonlinear vibrational analysis of the described plate is considered as an innovation of the present paper, which had not been done before. To model this problem, third-order shear deformation theory along with Gauss's laws for electrostatics and magnetostatics, first-order piston theory, and Galerkin and multiple times scale methods are used. After validating the presented method, effects of several parameters on the natural frequency, time history, backbone curve, and phase plane diagram of this smart composite plate are obtained. It is found that for plates with constant a/h ratio, electric and magnetic potentials have noticeable effects on the time histories, phase plane diagrams and backbone curves of the plates with smaller thicknesses. In addition, the numerical results of this research indicate that some parameters have considerable effect on the vibration behavior of presented plate. Elastic parameters of the foundation, applied electric and magnetic potentials, and environment temperature are important parameters in this analysis.

Keywords: Magneto-electro-elastic; Two-dimensional plate; Third-order plate theory; Nonlinear vibration; Aerodynamic loading.

1 INTRODUCTION

THE piezoelectric materials show coupling between mechanical and electrical fields whereas the piezomagnetic materials show coupling between mechanical and magnetic fields. However, Magneto-Electro-Elastic (MEE)

*Corresponding author.Tel.: +98 9141051582.
E-mail address: *soheilrazavi@outlook.com* (S.Razavi).

composites made with piezoelectric and piezomagnetic phases not only have the piezoelectric and piezomagnetic properties, but also exhibit magnetoelectric (ME) coupling effect which is not present in its constituents, which is why these materials have found a large application as sensors and actuators, medical ultrasonic imaging, etc. [1]. Pan [2] studied multilayered MEE plates analytically for the first time. Pan and Heyliger [3] determined the free vibration response of this smart plate. Ebrahimi et al. [4] presented a shear deformable plate model for free vibration analysis of FG MEE plates. Jiang and Heyliger [5] used a semi-analytical approach to evaluate thickness effects in the free vibration of laminated MEE plates under various lateral boundary conditions. Vinyas and Kattimani [6] studied the effect of hygrothermal environment on the free vibration characteristics of MEE plates based on a higher-order finite element method (FEM). Vinyas et al. [7] presented a TSDT-based FE model to study the free vibration behaviour of circular and annular MEE plates. Free vibration response of skew MEE plates using a third-order shear deformation plate theory (TSDT)-based FE model has also been studied [8]. Vinyas [9] evaluated the effect of active constrained layer damping on the linear frequency response of skew MEE plates based on a three-dimensional (3D) FE formulation. Zhou et al. [10] presented a cell-based smoothed FE model to simulate the transient responses of MEE structures. Daga et al. [1] studied the harmonic response of three-phase MEE beam under mechanical, electrical, and magnetic loads based on a FEM. Shooshtari and Razavi [11] obtained the vibration response of a MEE plate subjected to harmonic forces. Zhang et al. [12] presented closed-form solutions for vibrations of a MEE beam with variable cross section based on Timoshenko beam theory. MEE nano-structures have also been studied and their dynamic responses have been obtained. Mohammadimehr et al. [13] obtained the free vibration response of MEE curved panels reinforced by carbon nanotubes (CNTs) based on the first order shear deformation theory (FSDT). Kiani et al. [14] carried out the vibration response of MEE nanoplate made of functionally graded materials based on TSDT. Farajpour et al. [15] presented a scale-dependent continuum model to investigate the effect of initial in-plane edge displacement on the nonlinear vibration of MEE nanofilms. Vinyas [16] analyzed the free vibration of carbon nanotube-reinforced MEE plates based on a higher-order FEM. Xue et al. [17] obtained an analytical expression for the large deflection of a MEE thin plate for the first time. Razavi and Shooshtari [18] and Shooshtari and Razavi [19] studied the nonlinear vibrations of MEE rectangular plate and doubly-curved shell, respectively, for the first time. Shabanpour et al. [20] presented a nonlinear analytical model for the transverse vibration of laminated MEE plate based on the TSDT. Ansari et al. [21] used variational differential quadrature (VDQ) method to investigate the nonlinear free vibrations MEE plates under thermal environment.

Thin-walled structures are widely used in various branches of engineering, in particular in the aerospace industry. Therefore, one of the key factors in the design of these structures is the aerodynamic considerations. So, reliable mathematical modeling is crucial for understanding such phenomena and aiding aerospace structural design. Responses of thin-walled isotropic and composite structures subjected to aerodynamic loading have been discussed extensively. Carrera and Zappino [22] investigated the aeroelastic behaviour of pinched plates in supersonic flow changing with altitude by a finite number of points. Zhao and Zhang [23] presented the analysis of the nonlinear dynamics for a composite laminated cantilever rectangular plate subjected to the supersonic flow and the in-plane excitations using the third-order piston theory. Meijer and Dala [24] developed an aeroelastic prediction framework for cantilevered plates in supersonic flow using local piston theory and quasi-steady aerodynamic methodology and obtained good accuracy of flutter prediction at significantly reduced computation times. Chen et al. [25] carried out numerical simulations on the post-flutter response of a flexible cantilever plate by establishing a nonlinear aeroelastic model. Eugeni et al. [26] studied a nonlinear elastic plate in a supersonic unsteady flow forced by a dynamic excitation and a biaxial compressive load by using the piston theory including nonlinearities up to the third order. Pacheco et al. [27] employed a more realistic model for FE analysis of fluttering plates reinforced by flexible beams using the Mindlin and linear piston theories. Smart structures have also been studied and their responses to aerodynamic and electromagnetic loadings have been determined. Raja et al. [28] used multilayer piezoelectric actuators and sensors for constructing a linear quadratic Gaussian controller to suppress the flutter of a composite plate. Song and Li [29] studied the active aeroelastic flutter analysis and vibration control at the flutter bounds of the supersonic composite laminated plates with the piezoelectric patches using the supersonic piston theory. Makihara and Shimose [30] studied the harvesting of electrical energy generated from the flutter phenomenon of a plate wing. Leão et al. [31] investigated the possibility of increasing the supersonic flutter boundary of a composite flat panel by applying a multimode shunted piezoceramic in series topology. Lu et al. [32] introduced a nonlinear partial differential equation for the dynamic analysis of a cantilevered piezoelectric laminated composite plate, under the combined action of aerodynamic load and piezoelectric excitation. The static stability of a thin plate in axial subsonic airflow has also been studied [33]. Song et al. [34] presented a new active flutter control method which suppresses the flutter effectively and without affecting the natural frequency of the structural system based on the Kirchhoff plate theory and supersonic piston theory. Kelkar et al. [35] presented a concept for energy harvesting

system that uses free-play induced limit cycle oscillations as the energy resource and magnetostrictive device that can harness that energy in a 2-D aeroelastic system. The effects of the pseudo-elastic hysteresis of shape memory alloy springs on the aeroelastic behaviour of a typical airfoil section for different sets of alloy constitutive properties have also been investigated [36-38]. Rafiee et al. [39 and 40] studied nonlinear free and forced vibration of a piezoelectric composite shell under thermo-electro-aerodynamic loading. In numerous papers, Arefi and Zenkour [41-45] investigated thermo-electro-mechanical behavior of nonoplate using different theories in different conditions. Also, Arefi et al. [46] studied vibration nonlocal analysis of an elastic three-layered nanoplate with exponentially graded graphene sheet core and piezomagnetic face-sheets on Pasternak's foundation. They scrutinized the natural frequency for different side length ratio, nonlocal parameter, inhomogeneity parameter, and parameters of foundation numerically. In another study, Arefi and Soltan Arani [47] investigated nonlocal magneto-electro-thermo-elastic analysis of a functionally graded nanobeam subjected to magneto-electro-elastic loads using third-order shear deformation theory and derived the bending results for a simply supported nanobeam in terms of parameters of loadings, materials, and geometries.

To the author's knowledge, there is not any study about the nonlinear vibration response of MEE structures under magneto-electro-thermo-aerodynamic loading. So, this paper intends to fill this research gap. To this end, it is assumed that the MEE body is poled along the z direction and subjected to electric and magnetic potentials between the upper and lower surfaces. To model the problem, TSDT along with Gauss's laws for electrostatics and magnetostatics, first-order piston theory and Galerkin method and multiple times scale method are used. After validating the presented method, effects of several parameters on the nonlinear vibration response of this smart plate is studied.

2 DERIVING THE EQUATION OF MOTION

Based on Reddy's TSDT, the displacement field of a rectangular plate is expressed by [48]:

$$\begin{aligned} u(x,y,z,t) &= u_0(x,y,t) + z\,\theta_x(x,y,t) - \frac{4}{3h^2} z^3 \left(\theta_x + w_{0,x}\right) \\ v(x,y,z,t) &= v_0(x,y,t) + z\,\theta_y(x,y,t) - \frac{4}{3h^2} z^3 \left(\theta_y + w_{0,y}\right) \\ w(x,y,z,t) &= w_0(x,y,t) \end{aligned} \tag{1}$$

In which u_0, v_0, and w_0 are the displacements of the mid-surface along x, y, and z axes, respectively, and θ_x and θ_y are the rotations of a transverse normal about the y and x axes, respectively (Fig. 1).

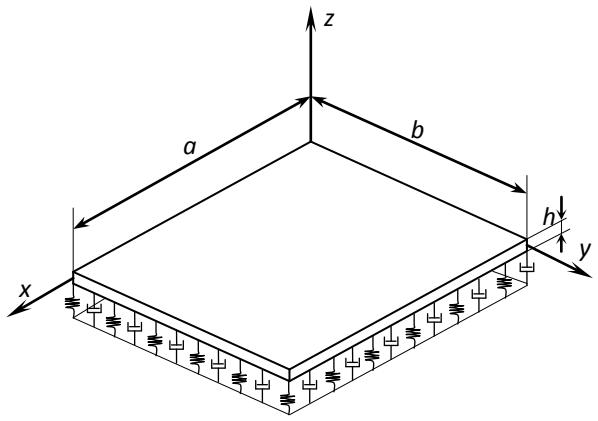

Fig.1
Geometry of a MEE rectangular resting on a damped elastic foundation.

Using the above displacement field, the linear strain-displacement relations are given as below [48]:

$$\begin{Bmatrix}\varepsilon_x\\ \varepsilon_y\\ \gamma_{yz}\\ \gamma_{xz}\\ \gamma_{xy}\end{Bmatrix}=\begin{Bmatrix}u_{0,x}+\frac{1}{2}w_{0,x}^{2}\\ v_{0,y}+\frac{1}{2}w_{0,y}^{2}\\ \theta_y+w_{0,y}\\ \theta_x+w_{0,x}\\ u_{0,y}+v_{0,x}+w_{0,x}w_{0,y}\end{Bmatrix}+z\begin{Bmatrix}\theta_{x,x}\\ \theta_{y,y}\\ 0\\ 0\\ \theta_{x,y}+\theta_{y,x}\end{Bmatrix}-\frac{4}{h^2}z^2\begin{Bmatrix}0\\ 0\\ \theta_y+w_{0,y}\\ \theta_x+w_{0,x}\\ 0\end{Bmatrix}-\frac{4}{3h^2}z^3\begin{Bmatrix}\theta_{x,x}+w_{0,xx}\\ \theta_{y,y}+w_{0,yy}\\ 0\\ 0\\ \theta_{x,y}+\theta_{y,x}+2w_{0,xy}\end{Bmatrix} \tag{2}$$

Assuming that the electric and magnetic fields are applied along z-direction, the constitutive equations of a transversely-isotropic MEE material can be written in the following form [49]:

$$\begin{Bmatrix}\sigma_x\\ \sigma_y\\ \tau_{yz}\\ \tau_{xz}\\ \tau_{xy}\end{Bmatrix}=\begin{bmatrix}C_{11}&C_{12}&0&0&0\\ C_{12}&C_{22}&0&0&0\\ 0&0&C_{44}&0&0\\ 0&0&0&C_{55}&0\\ 0&0&0&0&C_{66}\end{bmatrix}\begin{Bmatrix}\varepsilon_x\\ \varepsilon_y\\ \gamma_{yz}\\ \gamma_{xz}\\ \gamma_{xy}\end{Bmatrix}+\begin{bmatrix}0&0&e_{31}\\ 0&0&e_{32}\\ 0&e_{24}&0\\ e_{15}&0&0\\ 0&0&0\end{bmatrix}\begin{Bmatrix}0\\ 0\\ \phi_{,z}\end{Bmatrix}+\begin{bmatrix}0&0&q_{31}\\ 0&0&q_{32}\\ 0&q_{24}&0\\ q_{15}&0&0\\ 0&0&0\end{bmatrix}\begin{Bmatrix}0\\ 0\\ \psi_{,z}\end{Bmatrix}-\begin{Bmatrix}\beta_{11}\\ \beta_{22}\\ 0\\ 0\\ 0\end{Bmatrix}\Delta T \tag{3}$$

$$\begin{Bmatrix}D_x\\ D_y\\ D_z\end{Bmatrix}=\begin{bmatrix}0&0&0&e_{15}&0\\ 0&0&e_{24}&0&0\\ e_{31}&e_{32}&0&0&0\end{bmatrix}\begin{Bmatrix}\varepsilon_x\\ \varepsilon_y\\ \gamma_{yz}\\ \gamma_{xz}\\ \gamma_{xy}\end{Bmatrix}-\begin{bmatrix}\eta_{11}&0&0\\ 0&\eta_{22}&0\\ 0&0&\eta_{33}\end{bmatrix}\begin{Bmatrix}0\\ 0\\ \phi_{,z}\end{Bmatrix}-\begin{bmatrix}d_{11}&0&0\\ 0&d_{22}&0\\ 0&0&d_{33}\end{bmatrix}\begin{Bmatrix}0\\ 0\\ \psi_{,z}\end{Bmatrix}+\begin{Bmatrix}0\\ 0\\ p_z\end{Bmatrix}\Delta T \tag{4}$$

$$\begin{Bmatrix}B_x\\ B_y\\ B_z\end{Bmatrix}=\begin{bmatrix}0&0&0&q_{15}&0\\ 0&0&q_{24}&0&0\\ q_{31}&q_{32}&0&0&0\end{bmatrix}\begin{Bmatrix}\varepsilon_x\\ \varepsilon_y\\ \gamma_{yz}\\ \gamma_{xz}\\ \gamma_{xy}\end{Bmatrix}-\begin{bmatrix}d_{11}&0&0\\ 0&d_{22}&0\\ 0&0&d_{33}\end{bmatrix}\begin{Bmatrix}0\\ 0\\ \phi_{,z}\end{Bmatrix}-\begin{bmatrix}\mu_{11}&0&0\\ 0&\mu_{22}&0\\ 0&0&\mu_{33}\end{bmatrix}\begin{Bmatrix}0\\ 0\\ \psi_{,z}\end{Bmatrix}+\begin{Bmatrix}0\\ 0\\ m_z\end{Bmatrix}\Delta T \tag{5}$$

where $\{\boldsymbol{\sigma}\}$ and $\{\boldsymbol{\varepsilon}\}$ are stress and strain vectors, respectively; $\{\boldsymbol{D}\}$ and $\{\boldsymbol{B}\}$ are the electric displacement and magnetic flux density vectors, respectively; $\{\boldsymbol{E}\}=\{0\ \ 0\ -\phi_{,z}\}^T$ and $\{\boldsymbol{H}\}=\{0\ \ 0\ -\psi_{,z}\}^T$ are electric field and magnetic field vectors, respectively, where ϕ and ψ denote electric and magnetic potentials and which have been substituted into Eqs. (3)-(5); $[C_{ij}]$, $[\eta_{ij}]$ and $[\mu_{ij}]$ are the elastic, dielectric and magnetic permeability coefficient matrices, respectively; $[e_{ij}]$, $[q_{ij}]$ and $[d_{ij}]$ are the piezoelectric, piezomagnetic, and ME coefficient matrices, respectively; p_z, m_z and β_{ii} are pyroelectric, pyro-magnetic and thermal moduli, respectively; and ΔT denotes the temperature change.

Using Hamilton's principle and based on Reddy's TSDT, one can obtain the equations of motion of a rectangular plate resting on a damped elastic foundation as below [48]:

$$N_{x,x}+N_{xy,y}=I_0\ddot{u}_0+J_1\ddot{\phi}_x-c_1I_3\ddot{w}_{0,x} \tag{6a}$$

$$N_{xy,x}+N_{y,y}=I_0\ddot{v}_0+J_1\ddot{\phi}_y-c_1I_3\ddot{w}_{0,y} \tag{6b}$$

$$\begin{aligned}&\overline{Q}_{x,x}+\overline{Q}_{y,y}+\tfrac{4}{3h^2}\left(P_{x,xx}+2P_{xy,xy}+P_{y,yy}\right)+\left(N_xw_{0,x}+N_{xy}w_{0,y}\right)_{,x}+\left(N_{xy}w_{0,x}+N_yw_{0,y}\right)_{,y}\\ &-k_ww_0+k_s\nabla^2w_0-c_d\dot{w}_0-\Delta p=I_0\ddot{w}_0-\tfrac{16}{9h^4}I_6\left(\ddot{w}_{0,xx}+\ddot{w}_{0,yy}\right)+\tfrac{4}{3h^2}\left[J_4\left(\ddot{\theta}_{x,x}+\ddot{\theta}_{y,y}\right)+I_3\left(\ddot{u}_{0,x}+\ddot{v}_{0,y}\right)\right]\end{aligned} \tag{6c}$$

$$\overline{M}_{x,x}+\overline{M}_{xy,y}-\overline{Q}_x=J_1\ddot{u}_0+K_2\ddot{\theta}_x-\tfrac{4}{3h^2}J_4\ddot{w}_{0,x} \tag{6d}$$

$$\overline{M}_{xy,x}+\overline{M}_{y,y}-\overline{Q}_{y}=J_1\ddot{v}_0+K_2\ddot{\theta}_y-\tfrac{4}{3h^2}J_4\ddot{w}_{0,y} \tag{6e}$$

where k_w and k_s are spring and shear coefficients of the foundation, respectively, c_d is the damping coefficient of the foundation, and Δp is aerodynamic pressure passing over the top surface of the plate. Other parameters of these equations are defined as below:

$$\begin{aligned}
&\overline{M}_x=M_x-\tfrac{4}{3h^2}P_x,\quad \overline{M}_y=M_y-\tfrac{4}{3h^2}P_y,\quad \overline{M}_{xy}=M_{xy}-\tfrac{4}{3h^2}P_{xy},\\
&\overline{Q}_x=Q_x-\tfrac{4}{h^2}R_x,\qquad \overline{Q}_y=Q_y-\tfrac{4}{h^2}R_y,\\
&I_i=\int_{z_1}^{z_2}\rho_0(z)^i\,dz\qquad (i=0,1,\ldots,6),\\
&J_j=I_j-\tfrac{4}{3h^2}I_{j+2}\qquad (j=1,4)\\
&K_2=I_2-\tfrac{8}{3h^2}I_4+\tfrac{16}{9h^4}I_6
\end{aligned} \tag{7a}$$

In which the force and moment resultants are obtained by:

$$\begin{Bmatrix}N_{\alpha\beta}\\M_{\alpha\beta}\\P_{\alpha\beta}\end{Bmatrix}=\int_{-\frac{h}{2}}^{\frac{h}{2}}\sigma_{\alpha\beta}\begin{Bmatrix}1\\z\\z^3\end{Bmatrix}dz,\qquad \begin{Bmatrix}Q_\alpha\\R_\alpha\end{Bmatrix}=\int_{-\frac{h}{2}}^{\frac{h}{2}}\sigma_{\alpha z}\begin{Bmatrix}1\\z^2\end{Bmatrix}dz,\qquad (\alpha,\beta=x,y) \tag{7b}$$

Since the density of the plate (ρ_0) is constant, Eq. (7a) results in:

$$I_1=I_3=I_5=0,\qquad J_1=0 \tag{7c}$$

On the other hand, for most engineering applications of thin walled structures, in-plane inertias can be neglected [50]. So, Eqs. (6a)-(6e) are reduced to:

$$N_{x,x}+N_{xy,y}=0 \tag{8}$$

$$N_{xy,x}+N_{y,y}=0 \tag{9}$$

$$\begin{aligned}
&\overline{Q}_{x,x}+\overline{Q}_{y,y}+\tfrac{4}{3h^2}\left(P_{x,xx}+2P_{xy,xy}+P_{y,yy}\right)+\left(N_x w_{0,x}+N_{xy}w_{0,y}\right)_{,x}+\left(N_{xy}w_{0,x}+N_y w_{0,y}\right)_{,y}\\
&-k_w w_0+k_s\nabla^2 w_0-c_d\dot{w}_0-\Delta p=I_0\ddot{w}_0-\tfrac{16}{9h^4}I_6\left(\ddot{w}_{0,xx}+\ddot{w}_{0,yy}\right)+\tfrac{4}{3h^2}J_4\left(\ddot{\theta}_{x,x}+\ddot{\theta}_{y,y}\right)
\end{aligned} \tag{10}$$

$$\overline{M}_{x,x}+\overline{M}_{xy,y}-\overline{Q}_x=K_2\ddot{\theta}_x-\tfrac{4}{3h^2}J_4\ddot{w}_{0,x} \tag{11}$$

$$\overline{M}_{xy,x}+\overline{M}_{y,y}-\overline{Q}_y=K_2\ddot{\theta}_y-\tfrac{4}{3h^2}J_4\ddot{w}_{0,y} \tag{12}$$

To express Eqs. (8)-(12) in terms of displacements and rotations, the resultants are obtained from Eq. (7b) and Eq. (3). However, since in Eq. (3), $\phi_{,z}$ and $\psi_{,z}$ are unknown parameters and the constitutive Eq. (3)-(5) are coupled to each other, Eqs. (4) and (5) along with Gauss's laws for electrostatics and magnetostatics and in the absence of unpaired electric charge are used to obtain the analytical expressions for ϕ and ψ, that is:

$$D_{x,x}+D_{y,y}+D_{z,z}=0,\qquad B_{x,x}+B_{y,y}+B_{z,z}=0 \tag{13}$$

Substituting Eqs. (4) and (5) into Eq. (13), one obtains:

$$\begin{aligned}\phi_{,zz} &= (\lambda_1 A_3 + \lambda_2 A_1) z^2 + \lambda_1 A_4 + \lambda_2 A_2 \\ \psi_{,zz} &= (\lambda_1 A_1 + \lambda_3 A_3) z^2 + \lambda_1 A_2 + \lambda_3 A_4\end{aligned} \tag{14}$$

where

$$\begin{aligned}\lambda_1 &= d_{33} / (d_{33}^2 - \eta_{33}\mu_{33}) \\ \lambda_2 &= -\mu_{33} / (d_{33}^2 - \eta_{33}\mu_{33}) \\ \lambda_3 &= -\eta_{33} / (d_{33}^2 - \eta_{33}\mu_{33})\end{aligned} \tag{15}$$

$$\begin{aligned}A_1 &= -\tfrac{4}{h^2}\left[e_{24}(\theta_{x,y} + w_{0,xy}) + e_{31}(\theta_{x,x} + w_{0,xx}) + e_{15}(\theta_{y,x} + w_{0,xy}) + e_{32}(\theta_{y,y} + w_{0,yy})\right] \\ A_2 &= e_{24}(\theta_{x,y} + w_{0,xy}) + e_{15}(\theta_{y,x} + w_{0,xy}) + e_{31}\theta_{x,x} + e_{32}\theta_{y,y} \\ A_3 &= -\tfrac{4}{h^2}\left[q_{24}(\theta_{x,y} + w_{0,xy}) + q_{31}(\theta_{x,x} + w_{0,xx}) + q_{15}(\theta_{y,x} + w_{0,xy}) + q_{32}(\theta_{y,y} + w_{0,yy})\right] \\ A_4 &= q_{24}(\theta_{x,y} + w_{0,xy}) + q_{15}(\theta_{y,x} + w_{0,xy}) + q_{31}\theta_{x,x} + q_{32}\theta_{y,y}\end{aligned} \tag{16}$$

It is obvious from Eq. (14) that integrating these equations with respect to z, one can obtain potentials' distributions. So, integrating Eq. (14) with respect to z gives:

$$\begin{aligned}\phi_{,z} &= \tfrac{1}{3}(\lambda_1 A_3 + \lambda_2 A_1) z^3 + (\lambda_1 A_4 + \lambda_2 A_2) z + \phi_0 \\ \psi_{,z} &= \tfrac{1}{3}(\lambda_1 A_1 + \lambda_3 A_3) z^3 + (\lambda_1 A_2 + \lambda_3 A_4) z + \psi_0\end{aligned} \tag{17}$$

where ϕ_0 and ψ_0 are the constants of integration and are obtained by using the ME boundary conditions on the two surfaces of the plate. Assuming that The MEE body is poled along the z direction and subjected to an electric potential V_0 and a magnetic potential Ω_0 between the upper and lower surfaces of the plate, the ME boundary conditions are stated as below:

$$\begin{aligned}&\phi(x, y, z = -\tfrac{h}{2}) = \psi(x, y, z = -\tfrac{h}{2}) = 0, \\ &\phi(x, y, z = +\tfrac{h}{2}) = V_0, \quad \psi(x, y, z = +\tfrac{h}{2}) = \Omega_0\end{aligned} \tag{18}$$

which result in the following expressions for the gradients of electric and magnetic potentials:

$$\begin{aligned}\phi_{,z} &= \tfrac{1}{3}(\lambda_1 A_3 + \lambda_2 A_1) z^3 + (\lambda_1 A_4 + \lambda_2 A_2) z + \tfrac{V_0}{h} \\ \psi_{,z} &= \tfrac{1}{3}(\lambda_1 A_1 + \lambda_3 A_3) z^3 + (\lambda_1 A_2 + \lambda_3 A_4) z + \tfrac{\Omega_0}{h}\end{aligned} \tag{19}$$

The resultants are obtained by Eqs. (3), (7b) and (19):

$$N_x = h\left[C_{11}(u_{0,x} + \tfrac{1}{2}w_{0,x}^2) - \beta_{11}\Delta T\right] + e_{31}V_0 + q_{31}\Omega_0 \tag{20}$$

$$Q_x = \tfrac{2h}{3}C_{55}(w_{0,x} + \theta_x), \qquad R_x = \tfrac{h^2}{20}Q_x \tag{21}$$

$$\begin{aligned}M_x &= \tfrac{h^3}{60}(C_{11} + \lambda_2 e_{31}^2 + 2\lambda_1 e_{31} q_{31} + \lambda_3 q_{31}^2)\left[4\theta_{x,x} - w_{0,xx}\right] \\ P_x &= \tfrac{h^5}{1680}(C_{11} + \lambda_2 e_{31}^2 + 2\lambda_1 e_{31} q_{31} + \lambda_3 q_{31}^2)\left[16\theta_{x,x} - 5w_{0,xx}\right]\end{aligned} \tag{22}$$

where all terms involving y and v_0 are deleted in Eqs. (20)-(22) to obtain the equations of motion for a two-dimensional MEE plate [51]. Following the same procedure on Eqs. (8)-(12), on the other hand, gives the following equations of motion for a two-dimensional plate:

$$N_{x,x} = 0 \tag{23}$$

$$\overline{Q}_{x,x} + \tfrac{4}{3h^2} P_{x,xx} + \left(N_x w_{0,x}\right)_{,x} - k_w w_0 + k_s w_{0,xx} - c_a \dot{w}_0 - \Delta p = I_0 \ddot{w}_0 - \tfrac{16}{9h^4} I_6 \ddot{w}_{0,xx} + \tfrac{4}{3h^2} J_4 \ddot{\theta}_{x,x} \tag{24}$$

$$\overline{M}_{x,x} - \overline{Q}_x = K_2 \ddot{\theta}_x - \tfrac{4}{3h^2} J_4 \ddot{w}_{0,x} \tag{25}$$

where for high Mach numbers, the aerodynamic pressure loading Δp along the positive x direction is determined by [51]:

$$\Delta p = \Lambda_\infty \left(w_{0,x} + \Gamma_\infty \dot{w}_0\right) \tag{26}$$

where $\Lambda_\infty = \frac{\rho_\infty U_\infty^2}{\sqrt{M_\infty^2 - 1}}$ and $\Gamma_\infty = \frac{M_\infty^2 - 2}{M_\infty^2 - 1} \frac{1}{U_\infty}$ in which ρ_∞ is air density, U_∞ is flow velocity, and M_∞ is Mach number. Substituting Eqs. (2), (3), (7b) and (19) into Eqs. (23)-(25) gives:

$$u_{0,xx} + w_{0,x} w_{0,xx} = 0 \tag{27}$$

$$\begin{aligned} &\delta_1 w_{0,xxxx} + \delta_2 w_{0,xx} + \delta_3 w_{0,x} + \delta_4 w_0 + \delta_5 \theta_{x,xxx} + \delta_6 \theta_{x,x} + \delta_7 \dot{w}_0 + \\ &\quad \delta_8 u_{0,xx} w_{0,x} + \delta_8 u_{0,x} w_{0,xx} + \delta_9 w_{0,x}^2 w_{0,xx} = I_0 \ddot{w}_0 + \hat{I}_1 \ddot{w}_{0,xx} + \hat{I}_2 \ddot{\theta}_{x,x} \end{aligned} \tag{28}$$

$$\delta_{10} \theta_{x,xx} - \delta_6 \theta_x - \delta_5 w_{0,xxx} - \delta_6 w_{0,x} = K_2 \ddot{\theta}_x - \hat{I}_2 \ddot{w}_{0,x} \tag{29}$$

where the coefficients are given in Appendix A. To solve these set of nonlinear partial differential equations (PDEs), Eqs. (27) and (29) are solved to obtain u_0 and θ_x, respectively, in terms of w_0 and its derivatives:

$$u_{0,xx} = -w_{0,x} w_{0,xx}, \qquad \theta_x = \frac{\left(\delta_5 \frac{\partial^3}{\partial x^3} + \delta_6 \frac{\partial}{\partial x} - \hat{I}_2 \frac{\partial^3}{\partial x \partial t^2}\right)}{\left(\delta_{10} \frac{\partial^2}{\partial x^2} - \delta_6 - K_2 \frac{\partial^2}{\partial t^2}\right)} w_0 \tag{30}$$

Substituting Eq. (30) into Eq. (28) gives:

$$\begin{aligned} &\hat{L}_1 \ddot{w}_0 + \hat{L}_2 \dot{w}_0 + \hat{L}_3 w_0 + \hat{L}_4 w_{0,xx}^3 + \hat{L}_5 w_{0,x} w_{0,xx} w_{0,xxx} + \hat{L}_6 w_{0,x}^2 w_{0,xxxx} + \hat{L}_7 w_{0,x}^2 w_{0,xx} \\ &+ \hat{L}_8 w_{0,xt}^2 w_{0,xx} + \hat{L}_8 w_{0,x} w_{0,xx} w_{0,xtt} + \hat{L}_9 w_{0,x} w_{0,xt} w_{0,xxt} + \hat{L}_{10} w_{0,x}^2 w_{0,xxtt} = 0 \end{aligned} \tag{31}$$

where $\hat{L}_i \ (i = 1,2,3)$ and $\hat{L}_i \ (i = 4,5,\ldots,10)$ are differential and constant operators, respectively, which are defined in Appendix B.

For the simply-supported boundary condition, the transverse displacement can be expressed by:

$$w_0 = hW(t) \sin(\pi x / a) \tag{32}$$

Substituting Eq. (32) into Eq. (31) and using the orthogonality of trigonometric functions, one obtains the following ordinary differential equation (ODE) with cubic stiffness and inertial nonlinearities:

$$G_1 \ddot{W} + G_2 \dot{W} + G_3 W + G_4 W^3 + G_5 \ddot{W} W^2 + G_6 \dot{W}^2 W = 0 \tag{33}$$

where $G_i\ (i=1,2,\ldots,6)$ are constant coefficients which are given in Appendix C.

3 ANALYTICAL SOLUTION OF THE EQUATION OF MOTION

Defining the dimensionless time as:

$$\tau=\frac{1}{a^2}\sqrt{\frac{C_{11}h^3}{I_0}}t \tag{34}$$

and substituting it into Eq. (33), results in the following dimensionless nonlinear ODE:

$$W_{,\tau\tau}+\zeta W_{,\tau}+\omega^2 W+\alpha W^3+\beta W_{,\tau\tau}W^2+\gamma W_{,\tau}^2 W=0 \tag{35}$$

where ω is the dimensionless natural frequency of the MEE plate and all the coefficients are given in Appendix D. Multiple time scales method is used to solve Eq. (35) analytically. To use this method, a small, positive and dimensionless parameter (ε) must be introduced to be multiplied by the nonlinear and damping terms [52]. The coefficients of the nonlinear terms in Eq. (35) contain the term $(h/a)^2$, which is dimensionless and small. So $\varepsilon=(h/a)^2$ is used as the so-called positive dimensionless parameter. That is:

$$W_{,\tau\tau}+\omega^2 W+\varepsilon\left[\hat{\zeta}W_{,\tau}+\hat{\alpha}W^3+\hat{\beta}W_{,\tau\tau}W^2+\hat{\gamma}W_{,\tau}^2W\right]=0 \tag{36}$$

where $\hat{\zeta}=\zeta/\varepsilon$, $\hat{\alpha}=\alpha/\varepsilon$, $\hat{\beta}=\beta/\varepsilon$, and $\hat{\gamma}=\gamma/\varepsilon$.

Moreover, to use the method of multiple time scales, independent time variables are introduced according to [52]:

$$T_n=\varepsilon^n\tau \qquad \text{for} \qquad n=0,1 \tag{37}$$

and W can be presented by the following expansion:

$$W(\tau,\varepsilon)=W_0(T_0,T_1)+\varepsilon W_1(T_0,T_1)+O(\varepsilon^2) \tag{38}$$

where $O(\varepsilon^2)$ denotes the higher order terms in the expansion. Using Eq. (37), the derivatives with respect to τ are rewritten as below:

$$\begin{aligned}\frac{d}{d\tau}&=D_0+\varepsilon D_1\\ \frac{d^2}{d\tau^2}&=D_0^2+2\varepsilon D_0D_1\end{aligned} \tag{39}$$

where D_0 and D_1 denote $\partial/\partial T_0$ and $\partial/\partial T_1$ respectively.

Substituting Eqs. (38) and (39) into Eq. (36) and equating the coefficients of ε^0 and ε^1 to zero, one obtains:

$$D_0^2W_0+\omega^2W_0=0 \tag{40}$$

$$D_0^2W_1+\omega^2W_1=-2D_1D_0W_0-\hat{\zeta}D_0W_0-\hat{\alpha}W_0^3-\hat{\beta}W_0^2\left(D_0^2W_0\right)-\hat{\gamma}W_0\left(D_0W_0\right)^2 \tag{41}$$

The solution of Eq. (40) can be expressed as:

$$W_0 = X_1(T_1)\exp(i\omega T_0) + cc \tag{42}$$

where $X_1 = X_1(T_1)$ is an unknown complex function of T_1, and *cc* denotes the complex conjugate of the preceding terms.

Substituting Eq. (42) into Eq. (41) gives:

$$D_0^2 W_1 + \omega^2 W_1 = \left[-2i\omega X_1' - \hat{\zeta} i\omega X_1 + \left(3\hat{\beta}\omega^2 - 3\hat{\alpha} - \hat{\gamma}\omega^2\right) X_1^2 \bar{X}_1\right]\exp(i\omega T_0) + \left(\hat{\beta}\omega^2 - \hat{\alpha} + \hat{\gamma}\omega^2\right) X_1^3 \exp(3i\omega T_0) + cc \tag{43}$$

where X_1' denotes dX_1/dT_1, and $\bar{X}_1$ is the complex conjugate of X_1. To have a periodic solution for W_1, the coefficients of $\exp(i\omega T_0)$ should be eliminated from Eq. (43), that is:

$$-2i\omega X_1' - \hat{\zeta} i\omega X_1 + \left(3\hat{\beta}\omega^2 - 3\hat{\alpha} - \hat{\gamma}\omega^2\right) X_1^2 \bar{X}_1 = 0 \tag{44}$$

Defining X_1 in polar form, that is $X_1 = \frac{1}{2} p \exp(iq)$, where p and q are real functions of T_1, and then by following the procedure described by Shooshtari and Razavi [53], the following closed-form expression is obtained for W:

$$W = p_0 \exp\left(-\tfrac{1}{2}\hat{\zeta}\varepsilon\tau\right)\cos\left[\left(\omega - \tfrac{1}{8\omega}\varepsilon\hat{A}p_0^2\right)\tau + \hat{B} + q_0\right] \tag{45}$$

which is obtained by considering only the first term in expansion of W given in Eq. (38). In Eq. (45), p_0 and q_0 are constants, $\hat{A} = 3\hat{\beta}\omega^2 - 3\hat{\alpha} - \hat{\gamma}\omega^2$, and $\hat{B} = \frac{1}{8\omega\zeta}\hat{A}p_0^2$. The transverse displacement (w_0) of any point of the plate can be obtained by substituting Eq. (45) into Eq. (32). In addition, the nonlinear frequency ratio of the MEE plate is obtained as below:

$$\omega_{NL}/\omega = \left[1 - \left(\tfrac{h}{2a\omega}\right)^2 \hat{A}p_0^2\right]^{1/2} \tag{46}$$

where ω_{NL} denotes the nonlinear frequency of the plate.

4 NUMERICAL EXAMPLES AND DISCUSSION

In this section, the results which are obtained from the relations of present work have been compared with the results of previously published papers for isotropic and piezoelectric plates. For the considered isotropic thin plate, dimensionless natural frequency is determined using $\omega_n a^2\sqrt{\rho_0 h/D}$ in which $D = Eh^3/\left[12\left(1-\nu^2\right)\right]$ and $\omega_n = \sqrt{G_3/G_1}$, where E is Young modulus and ν is Poisson's ratio. The piezoelectric plate, on the other hand, is a thick plate with $a = 0.04\ m$ and $h = 0.01\ m$. The dimensionless natural frequency for this plate is obtained by $\omega_n\left(a^2/h\right)\sqrt{\rho_0/C_{11}}$. Material properties of the piezoelectric plate are given in Ramirez et al. [54]. The results are shown in Table 1. It is seen that there is good agreement between the results. The discrepancy between the results of PZT-4 plate is due to this fact that the plate is a quite thick one with $a/h = 4$, and on the other hand, in ref. [54] a 3D theory has been used to model the plate which obviously gives more accurate results for thick plates.

Table 1
Comparison of dimensionless natural frequencies of two-dimensional rectangular plates.

Method	Plate	
	isotropic	PZT-4
Young and Budynas [55]	9.8700	-
Ramirez et al. [54]	-	2.2650
Present study	9.8692	2.4218

Next, the linear and nonlinear free vibration of a simply-supported MEE two-dimensional rectangular to magneto-electro-thermo-aerodynamic loading is analyzed. Material properties of the studied MEE plate are given in Table 2.

Table 2
Material properties of $BaTiO_3$-$CoFe_2O_4$ composite material [56].

Properties	Values
Elastic [GPa]	$C_{11}=226,\quad C_{55}=44.2$
Piezoelectric [C/m^2]	$e_{31}=-2.2,\quad e_{15}=5.8$
Dielectric [$\times10^{-9}$ $C/(Vm)$]	$\eta_{33}=6.35$
Piezomagnetic [$N/(Am)$]	$q_{31}=290.1,\quad q_{15}=275$
Magnetoelectric [$\times10^{-12}$ $Ns/(CV)$]	$d_{33}=2737.5$
Magnetic [$\times10^{-6}$ Ns^2/C^2]	$\mu_{33}=83.5$
Thermal modulus [$\times10^{5}$ $N/(m^2K)$]	$\beta_{11}=4.74$
Pyroelectric [$\times10^{-6}$ C/N]	$p_z=25$
Pyromagnetic [$\times10^{-6}$ $N/(AmK)$]	$m_z=5.19$
Mass density [kg/m^3]	$\rho_0=5550$

To study the effects of aerodynamic loading on the response of the MEE plate, the following dimensionless parameters are defined:

$$\mu=\rho_\infty a/(\rho_0 h),\qquad \chi=\rho_\infty U_\infty^2 a^3/(\kappa C_{11}h^3) \tag{47}$$

where μ is mass ratio, χ is dimensionless aerodynamic pressure, and $\kappa=\sqrt{M_\infty^2-1}$.

4.1 Linear vibration

Effects of electric and magnetic potentials on the natural frequency have been studied and the results are shown in Tables 3 and 4. The thickness of the plate is changed while its length-to-thickness ratio (a/h) is constant for all the cases. It is seen that negative electric potentials and positive magnetic potentials increase the natural frequency of a MEE plate. This phenomenon can be useful to avoid the resonance in the forced vibration. Moreover, it is noticed that for plates with smaller thicknesses, the electric and magnetic potentials have more effect on the response of the plate.

Table 3
Effects of applied electric potential on the dimensionless frequency $\omega=100\omega_n a\sqrt{\rho_0/C_{11}}$ of a two-dimensional MEE plate ($a/h=20$).

h (mm)	V_0 (10^2V)		
	−1	0	+1
0.1	14.2279	14.1942	14.1604
1	14.1976	14.1942	14.1908
10	14.1945	14.1942	14.1939

Table 4

Effects of applied magnetic potential on the dimensionless frequency $\omega = 100\omega_n a\sqrt{\rho_0/C_{11}}$ of a two-dimensional MEE plate ($a/h = 20$).

h (mm)	Ω_0 ($10A$)		
	-1	0	$+1$
0.1	13.7416	14.1942	14.6328
1	14.1496	14.1942	14.2387
10	14.1897	14.1942	14.1987

Fig. 2 shows the effect of dimensionless foundation parameters on the dimensionless frequency $\omega = 100\omega_n a\sqrt{\rho_0/C_{11}}$ of a MEE plate with $a/h = 50$. The dimensionless foundation parameters are obtained by $K_s = k_s a^2/\left(C_{11}h^3\right)$ and $K_w = k_w a^4/\left(C_{11}h^3\right)$. It is seen that the dimensionless shear coefficient (K_s) has more effect on the natural frequency compared with the effect of the dimensionless spring coefficient (K_w). Moreover, it is seen that the relationships between the natural frequency and the foundation parameters are nonlinear.

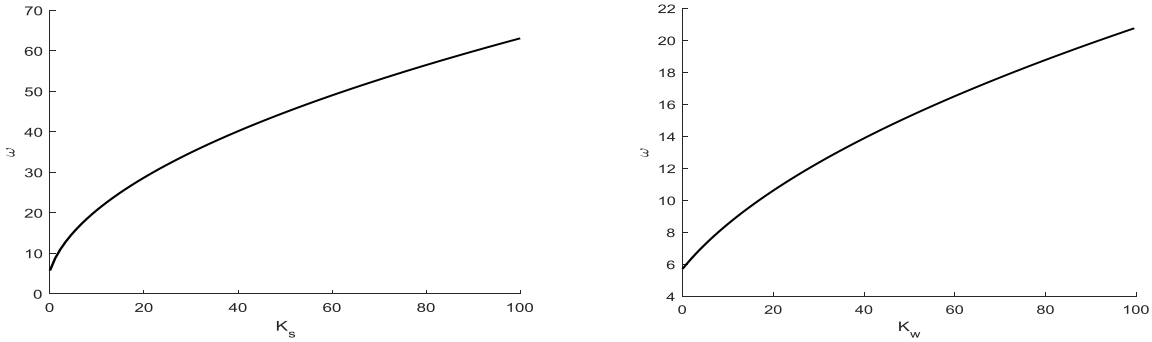

(a) (b)

Fig.2

Effects of elastic parameters of the foundation on the natural frequency of MEE plate: (a) $K_w = 0$, and (b) $K_s = 0$. ($V_0 = \Omega_0 = \Delta T = 0$).

Effect of temperature change on the natural frequency of a MEE plate has also been investigated and the result is shown in Fig. 3. The dimensionless frequency of the MEE plate is obtained by $\omega = 100\omega_n a\sqrt{\rho_0/C_{11}}$. It is observed that increasing the environment temperature decreases the stiffness of the system, and consequently decreases the natural frequency of the plate.

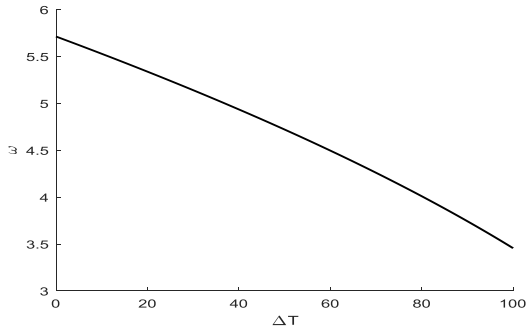

Fig.3

Effect of temperature rise on the natural frequency of a MEE plate. ($K_s = K_w = V_0 = \Omega_0 = 0$, $a/h = 50$).

To study the effects of aerodynamic pressure on the linear response of the plate, linear form of Eq. (33) should be solved analytically or numerically. If Eq. (33) is rewritten in the following linear form

$$\ddot{W} + 2\zeta\omega_n\dot{W} + \omega_n^2 W = 0 \tag{48}$$

where $\zeta = \dfrac{G_2}{2\sqrt{G_1 G_3}}$ is the damping ratio, the response of the plate in terms of time (t) is obtained as below:

$$W = e^{-\zeta\omega_n t}\left[W(0)\cos(\omega_d t) + \frac{\dot{W}(0)+\zeta\omega_n W(0)}{\omega_d}\sin(\omega_d t)\right] \tag{49}$$

where $\omega_d = \omega_n\sqrt{1-\zeta^2}$ is damped natural frequency; and $W(0)$ and $\dot{W}(0)$ are initial displacement and velocity, respectively.

Fig. 4 shows the time history of a MEE plate with and without considering aerodynamic damping. a/h is taken as 50 whiles $h = 1mm$. For both cases a closed-circuit ME boundary condition is considered and the temperature change and foundation parameters are taken as zero, that is $V_0 = \Omega_0 = \Delta T = k_s = k_w = c_d = 0$. It is clearly observed that the MEE plate without considering aerodynamic damping (i.e., when $\mu/M_\infty = 0$), is dependent on the initial value of $W = W(t)$ at $t = 0$. However, for the plate with aerodynamic damping, the response is independent of the initial condition and gradually decays to zero.

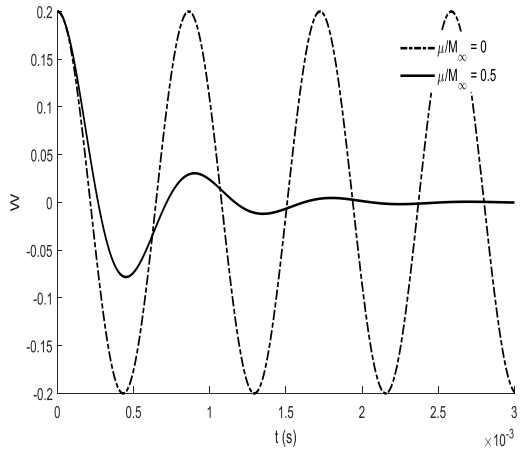

Fig.4
Linear time history of a MEE plate with aerodynamic damping and without aerodynamic damping ($\chi = 100,\ M_\infty = 1.5, W(0) = 0.2, \dot{W}(0) = 0$).

Effects of electric and magnetic potentials on the response of the same MEE plate with a/h = 100, h = 0.1 *mm* and $\mu/M_\infty = 0$ are also studied and the results are shown in Figs. 5 and 6, respectively. It is noticed that for positive electric potential, damped frequency decreases whereas the converse happens when applying the positive magnetic potential. Moreover, positive electric potential and negative magnetic potential decrease the amplitude of motion. So applying the positive electric potential or negative magnetic potential can be served as a way to increase the stability of the plate under aerodynamic pressure.

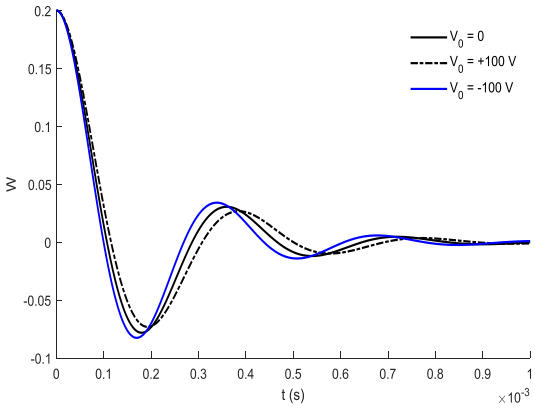

Fig.5
Effect of Electric potential on the linear time history of a MEE plate.

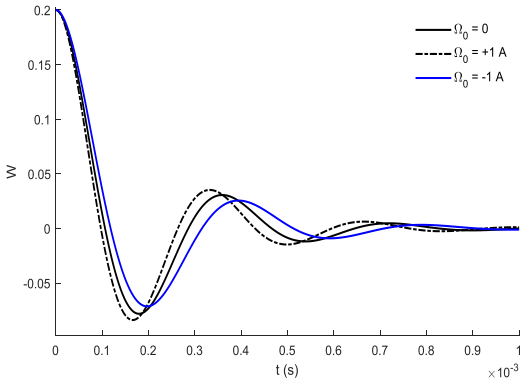

Fig.6
Effect of magnetic potential on the linear time history of a MEE plate.

Based on the relation given for G_2 in Appendix C, if

$$\frac{M_\infty^2-2}{\left(M_\infty^2-1\right)^{3/2}}+\frac{c_d}{\rho_\infty U_\infty}<0 \tag{50}$$

Is satisfied, the linear response of the plate will be unstable. Fig. 7 demonstrates the stable and unstable regions for $h=1mm$. In this figure, both axes are dimensionless parameters where $C_\infty=c_d\left/\left(\rho_\infty U_\infty h^2\right)\right.$. Unstable solution is the solution where the response grows continuously with time. For the studied MEE plate with positive foundation damping, the unstable solution may occur in Mach numbers smaller than $\sqrt{2}=1.4142$.

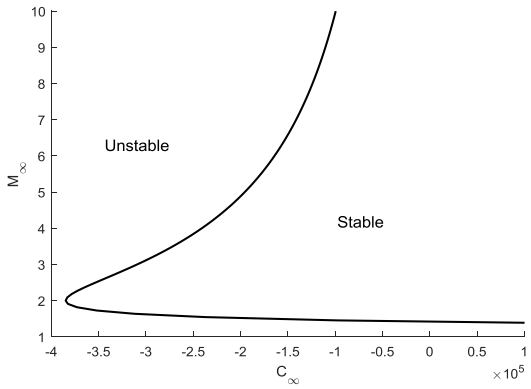

Fig.7
Stable and unstable solutions for different values of aerodynamic loading and foundation damping.

4.2 Nonlinear vibration

Fig. 8 shows the responses of a MEE plate with $a/h=100$ and $h=0.01m$, with and without considering aerodynamic damping. For both cases a closed-circuit ME boundary condition is considered and the temperature change and foundation parameters are taken as zero, that is $V_0=\Omega_0=\Delta T=k_s=k_w=c_d=0$. It is clearly observed that the MEE plate without considering aerodynamic damping (i.e., when $\mu/M_\infty=0$), is dependent on the initial value of $W=W(\tau)$ at $\tau=0$. However, for the plate with aerodynamic damping, the response is independent of the initial condition and gradually decays to zero.

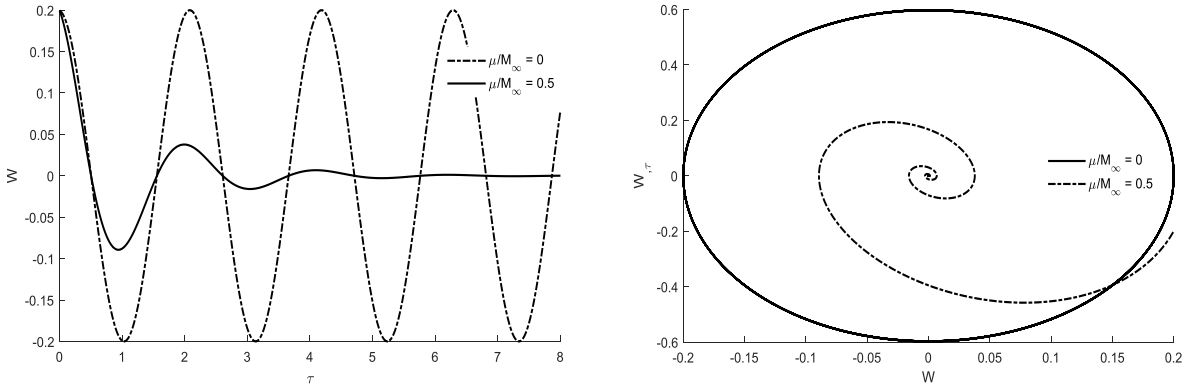

(a) (b)

Fig.8

(a) Time histories, and (b) phase plane diagrams of a MEE plate; with aerodynamic damping ($\mu/M_\infty = 0.5$) and without aerodynamic damping ($\mu/M_\infty = 0$). (For both cases; $\chi = 100$, $M_\infty = 1.5$, $W(0) = 0.2$).

Effects of electric and magnetic potentials on the response of the have also been studied and the results are shown in Fig. 9. The length-to-thickness ratio (a/h) is 100 ($h = 0.1mm$), $\Delta T = k_s = k_w = c_d = 0$, $\chi = 100$, $M_\infty = 1.5$, and $\mu/M_\infty = 0.5$. It is seen that positive electric potentials and negative magnetic potentials decrease the amplitude and the frequency of the plate.

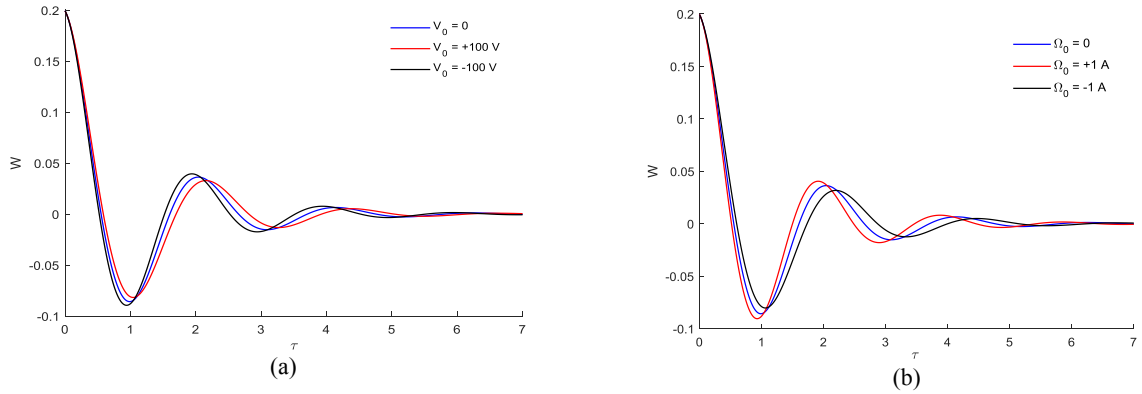

(a) (b)

Fig.9

Effects of: (a) electric ($\Omega_0 = 0$), and (b) magnetic ($V_0 = 0$) potentials on the time history response of a MEE plate ($W(0) = 0.2$).

Effects of foundation parameters, temperature change, Mach number and aerodynamic pressure on the time history of a MEE plate with $a/h = 50$ and $h = 0.01m$ have also been investigated. Fig.10 shows the results, in which the dimensionless foundation parameters are obtained by $K_s = k_s a^2 / (C_{11} h^3)$ and $K_w = k_w a^4 / (C_{11} h^3)$. For all the cases $\mu/M_\infty = 0.5$, $V_0 = \Omega_0 = c_d = 0$ and $W(0) = 0.2$ are considered. It is seen that elastic parameters of the foundation increase the frequency of the response which is the consequence of the increase in the stiffness of the system. In addition, it is noticed that K_s has more effect on the response compared with the effect of K_w. The converse happens when increasing the temperature. That is, positive temperature change decreases the stiffness and the frequency of the plate. Moreover, it is seen that higher Mach numbers and dimensionless aerodynamic pressure make the response to decay sooner.

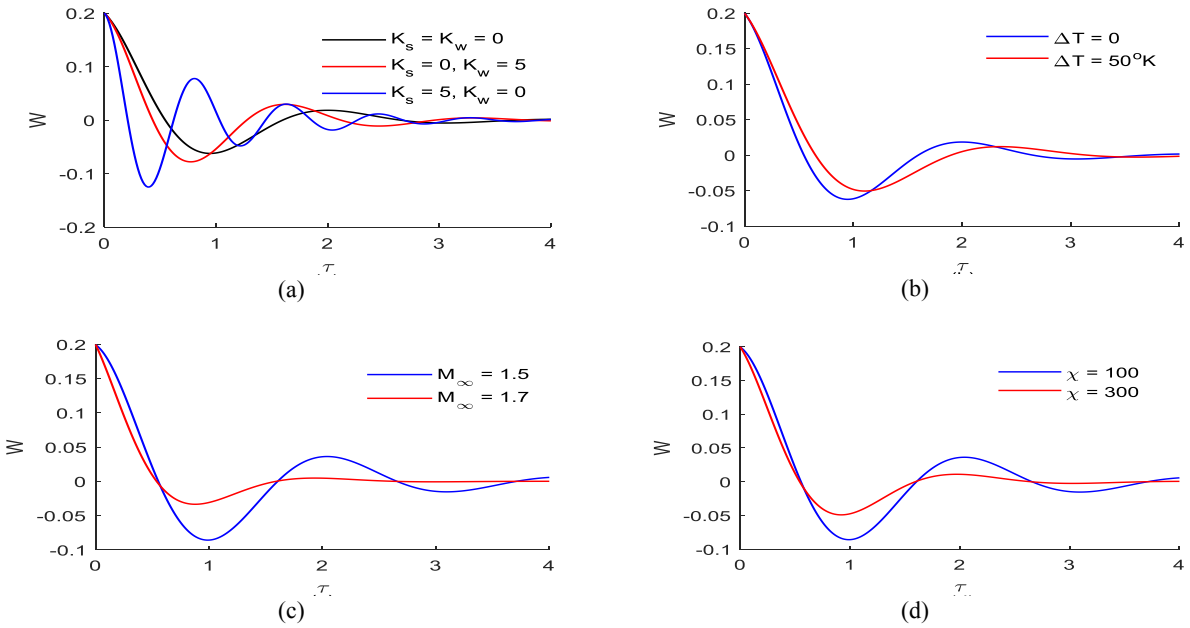

Fig.10
Effects of: (a) foundation parameters ($\chi = 100,\ M_\infty = 1.5,\ \Delta T = 0$), (b) temperature change ($\chi = 100,\ M_\infty = 1.5,\ K_s = K_w = 0$), (c) Mach number ($\chi = 100,\ \Delta T = K_s = K_w = 0$), and (d) dimensionless aerodynamic pressure ($M_\infty = 1.5,\ \Delta T = K_s = K_w = 0$) on the time history response of a MEE plate.

Effects of electric and magnetic potentials on the time history and phase plane diagram of a MEE plate with $a/h = 100$ while the thickness is changed have been investigated, too. It is seen from Figs. 11 and 12 that for plates with smaller thicknesses, potentials have noticeable effects on the response of the MEE plate.

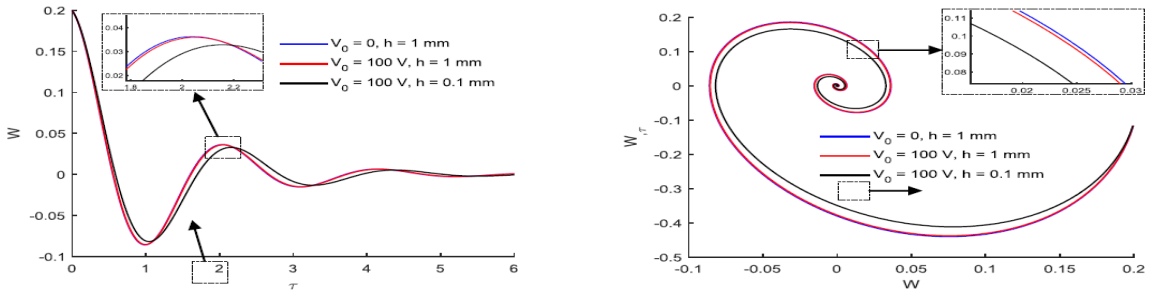

Fig.11
Effects of electric potential on the time history and phase plane plot of a MEE plate with different thicknesses ($\Delta T = K_w = K_s = c_d = \Omega_0 = 0,\ a/h = 100,\ \chi = 100,\ M_\infty = 1.5,\ \mu/M_\infty = 0.5$).

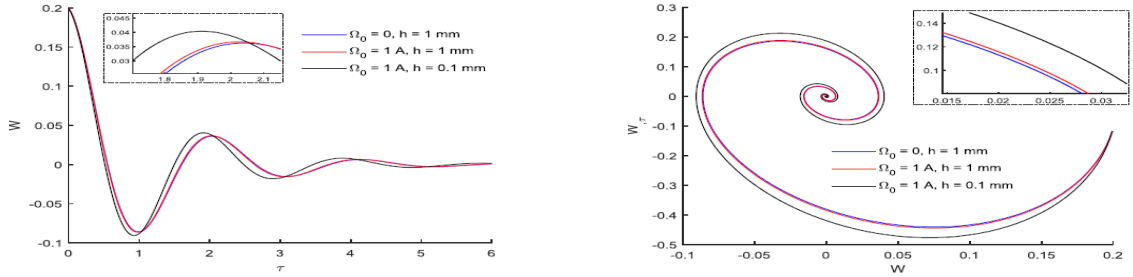

Fig.12
Effects of magnetic potential on the time history and phase plane plot of a MEE plate with different thicknesses ($\Delta T = K_w = K_s = c_d = V_0 = 0,\ a/h = 100,\ \chi = 100,\ M_\infty = 1.5,\ \mu/M_\infty = 0.5$).

Fig. 13 shows the backbone curves for a MEE plate with $c_d = 0$, $a/h = 100$, $\chi = 100$, $M_\infty = 1.5$, and $\mu/M_\infty = 0.5$. For Figs. 13(a) – (d), $h = 0.1mm$. It is seen that for some values of electric and magnetic potentials, the hardening nonlinearity changes to the softening one. This behaviour is also seen for higher temperature changes. Fig. 13(c) shows that using an elastic foundation decreases the nonlinearity of the system. It is also observed that K_s has more effect on the response compared with the effect of K_w. In Figs. 13(e) and 13(f) the value of thickness is changed while the a/h ratio is remained constant. It is noticed that the electric and magnetic potentials have more effect on the backbone curves of a MEE plate with smaller thickness.

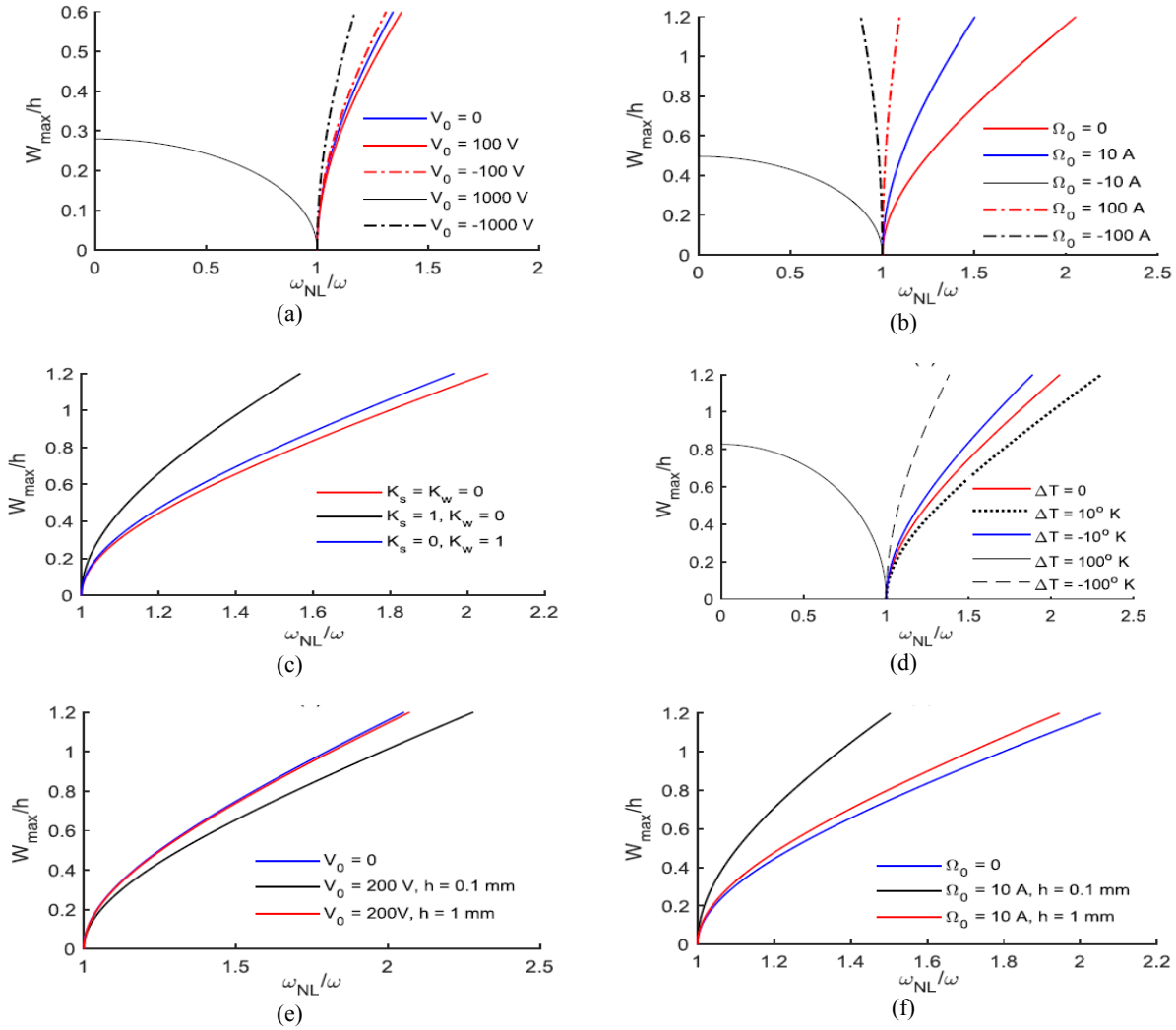

Fig.13
Backbone curves of a MEE plate for different: (a) electric potentials ($\Delta T = K_w = K_s = \Omega_0 = 0$), (b) magnetic potentials ($\Delta T = K_w = K_s = V_0 = 0$), (c) elastic parameters of the foundation ($\Delta T = \Omega_0 = V_0 = 0$), (d) temperature changes ($K_w = K_s = V_0 = \Omega_0 = 0$), and (e, f) thicknesses ($\Delta T = K_w = K_s = 0$).

Linear and nonlinear time histories have also been compared with each other. For nonlinear response, the curves have been obtained based on Eq. (38) considering one or two terms in the expansion. It is obvious from Fig. 14 that nonlinear response has higher frequency which is due to the effect of initial amplitude on the nonlinear frequency. Moreover, it is noticed that in Eq. (38), the first term is dominant in the time history which is why the two nonlinear time histories are almost the same.

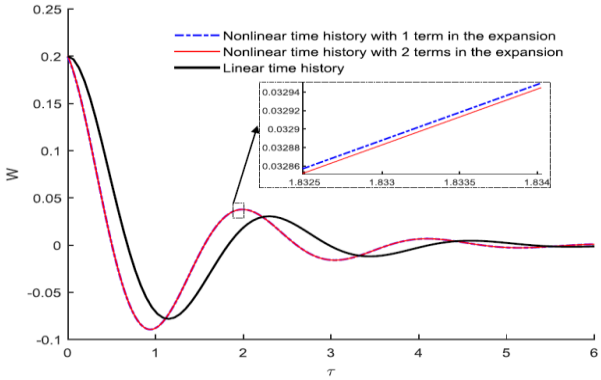

Fig.14
Comparison of linear and nonlinear time histories.

5 CONCLUSIONS

Linear and nonlinear vibration response of a two-dimensional MEE plate is studied analytically in this paper. The plate is under aerodynamic pressure and subjected to temperature change, and electric and magnetic potentials between the upper and lower surfaces. To model the problem, TSDT, Gauss's laws for electrostatics and magnetostatics, first-order piston theory, and Galerkin method and a perturbation method are used. By presenting some numerical examples it is found that:

- Elastic parameters of the foundation have nonlinear effects on the natural frequency. Moreover, they increase the frequency of the response which is the consequence of the increase in the stiffness of the system.
- Positive electric potentials and negative magnetic potentials decrease the natural frequency as well as the response amplitude and the nonlinear frequency of the MEE plate.
- Increasing the environment temperature decreases the stiffness and consequently decreases the natural frequency and nonlinear frequency of the MEE plate.
- Applying the positive electric potential or negative magnetic potential can be served as a way to increase the stability of the plate under aerodynamic pressure.
- The nonlinear time history of the MEE plate without considering aerodynamic damping is dependent on the initial displacement. However, for the plate with aerodynamic damping, the response is independent of the initial condition and gradually decays to zero.
- For plates with constant *a*/*h* ratio, electric and magnetic potentials have noticeable effects on the time histories, phase plane diagrams and backbone curves of the plates with smaller thicknesses.
- Generally, the MEE plate exhibits hardening behaviour. However, for some values of electric and magnetic potentials and temperature changes, the nonlinearity is of softening type.

APPENDIX A

$$\delta_1=-\tfrac{h^3}{252}\left(C_{11}+\lambda_2 e_{31}^2+2\lambda_1 e_{31}q_{31}+\lambda_3 q_{31}^2\right)\ ,\ \delta_2=\left[\tfrac{8}{15}C_{55}h+\left(e_{31}V_0+q_{31}\Omega_0-\beta_{11}h\Delta T\right)+k_s\right],$$

$$\delta_3=-\Lambda_\infty\ \ ,\ \ \delta_4=-k_w\ ,\ \delta_5=\tfrac{4h^3}{315}\left(C_{11}+\lambda_2 e_{31}^2+2\lambda_1 e_{31}q_{31}+\lambda_3 q_{31}^2\right),\ \delta_6=\tfrac{8}{15}C_{55}h\ \ ,$$

$$\delta_7=-\left(c_d+\Lambda_\infty\Gamma_\infty\right)\ ,\ \delta_8=hC_{11}\ ,\ \ \delta_9=\tfrac{3}{2}\delta_8\ ,\ \ \delta_{10}=\tfrac{17h^3}{315}\left(C_{11}+\lambda_2 e_{31}^2+2\lambda_1 e_{31}q_{31}+\lambda_3 q_{31}^2\right),$$

$$\hat{I}_1=-\tfrac{1}{252}\rho_0 h^3\ ,\ \ \hat{I}_2=\tfrac{4}{315}\rho_0 h^3$$

APPENDIX B

$$\hat{L}_1=\delta_6 I_0-\delta_4 K_2-\delta_3 K_2\frac{\partial}{\partial x}+\left(\delta_6\hat{I}_1-\delta_{10}I_0-2\delta_6\hat{I}_2-\delta_2 K_2\right)\frac{\partial^2}{\partial x^2}-\left(2\delta_5\hat{I}_2+\delta_{10}\hat{I}_1+\delta_1 K_2\right)\frac{\partial^4}{\partial x^4}$$

$$\hat{L}_2 = \delta_7\delta_{10}\frac{\partial^2}{\partial x^2} - \delta_6\delta_7$$

$$\hat{L}_3 = -\delta_4\delta_6 - \delta_3\delta_6\frac{\partial}{\partial x} + \left(\delta_6^2 - \delta_2\delta_6 + \delta_4\delta_{10}\right)\frac{\partial^2}{\partial x^2} + \delta_3\delta_{10}\frac{\partial^3}{\partial x^3} + \left(\delta_2\delta_{10} + 2\delta_5\delta_6 - \delta_1\delta_6\right)\frac{\partial^4}{\partial x^4} + \left(\delta_5^2 + \delta_1\delta_{10}\right)\frac{\partial^6}{\partial x^6}$$

$$\hat{L}_4 = 2\delta_8\delta_{10}\ ,\quad \hat{L}_5 = 3\hat{L}_4\ ,\quad \hat{L}_6 = \hat{L}_4/2\ ,\quad \hat{L}_7 = -\delta_8\delta_6\ ,\quad \hat{L}_8 = -2\delta_8K_2\ ,\quad \hat{L}_9 = 2\hat{L}_8\ ,\quad \hat{L}_{10} = \hat{L}_8/2$$

APPENDIX C

$$G_1 = \tfrac{1}{2}\delta_6 ahI_0 - \tfrac{1}{2}\delta_4 ahK_2 + \tfrac{1}{2a}\delta_{10}\pi^2 hI_0 - \tfrac{1}{2a}\delta_6\pi^2 h\hat{I}_1 + \tfrac{1}{a}\delta_6\pi^2 h\hat{I}_2 - \tfrac{1}{a^3}\delta_5\pi^4 h\hat{I}_2 - \tfrac{1}{2a^3}\delta_{10}\pi^4 h\hat{I}_1 + \tfrac{1}{2a}\delta_2\pi^2 hK_2 - \tfrac{1}{2a^3}\delta_1\pi^4 hK_2$$

$$G_2 = -\tfrac{1}{2}\delta_6\delta_7 ah - \tfrac{1}{2a}\delta_7\delta_{10}\pi^2 h$$

$$G_3 = -\tfrac{1}{2}\delta_4\delta_6 ah - \tfrac{1}{2a}\delta_6^2\pi^2 h - \tfrac{1}{2a^5}\delta_5^2\pi^6 h + \tfrac{1}{2a}\delta_2\delta_6\pi^2 h - \tfrac{1}{2a^3}\delta_1\delta_6\pi^4 h - \tfrac{1}{2a}\delta_4\delta_{10}\pi^2 h + \tfrac{1}{a^3}\delta_5\delta_6\pi^4 h + \tfrac{1}{2a^3}\delta_2\delta_{10}\pi^4 h - \tfrac{1}{2a^5}\delta_1\delta_{10}\pi^6 h$$

$$G_4 = \tfrac{1}{8a^5}\hat{L}_5\pi^6 h^3 - \tfrac{3}{8a^5}\hat{L}_4\pi^6 h^3 - \tfrac{1}{8a^3}\hat{L}_7\pi^4 h^3 + \tfrac{1}{8a^5}\hat{L}_6\pi^6 h^3$$

$$G_5 = -\tfrac{1}{8a^3}\hat{L}_8\pi^4 h^3 - \tfrac{1}{8a^3}\hat{L}_{10}\pi^4 h^3$$

$$G_6 = -\tfrac{1}{8a^3}\hat{L}_8\pi^4 h^3 - \tfrac{1}{8a^3}\hat{L}_9\pi^4 h^3$$

APPENDIX D

$$\zeta = a^2\frac{G_2}{G_1}\sqrt{\frac{I_0}{C_{11}h^3}}\ ,\quad \omega^2 = \frac{a^4 I_0 G_3}{C_{11}h^3 G_1}\ ,\quad \alpha = \frac{a^4 I_0 G_4}{C_{11}h^3 G_1}\ ,\quad \beta = G_5/G_1\ ,\quad \gamma = G_6/G_1$$

REFERENCES

[1] Daga A., Ganesan N., Shankar K., 2009, Harmonic response of three-phase magneto-electro-elastic beam under mechanical, electrical and magnetic environment, *Journal of Intelligent Material Systems and Structures* **20**: 1203-1220.

[2] Pan E., 2001, Exact solution for simply supported and multilayered magneto-electro-elastic plates, *Journal of Applied Mechanics* **68**: 608-618.

[3] Pan E., Heyliger P.R., 2002, Free vibrations of simply supported and multilayered magneto-electro-elastic plates, *Journal of Sound and Vibration* **252**: 429-442.

[4] Ebrahimi F., Jafari A., Barati M.R., 2017, Vibration analysis of magneto-electro-elastic heterogeneous porous material plates resting on elastic foundations, *Thin-Walled Structures* **119**: 33-46.

[5] Jiang C., Heyliger P.R., 2017, Thickness effects in the free vibration of laminated magnetoelectroelastic plates, *Journal of Mechanics of Materials and Structures* **12**: 521-544.

[6] Vinyas M., Kattimani S.C., 2018, Finite element evaluation of free vibration characteristics of magneto-electro-elastic rectangular plates in hygrothermal environment using higher-order shear deformation theory, *Composite Structures* **202**: 1339-1352.

[7] Vinyas M., Sandeep A.S., Nguyen-Thoi T., Ebrahimi F., Duc D.N., 2019, A finite element–based assessment of free vibration behaviour of circular and annular magneto-electro-elastic plates using higher order shear deformation theory, *Journal of Intelligent Material Systems and Structures* **30**: 2478-2501.

[8] Vinyas M., Nischith G., Loja M.A.R., Ebrahimi F., Duc N.D., 2019, Numerical analysis of the vibration response of skew magneto-electro-elastic plates based on the higher-order shear deformation theory, *Composite Structures* **214**: 132-142.

[9] Vinyas M., 2019, Vibration control of skew magneto-electro-elastic plates using active constrained layer damping, *Composite Structures* **208**: 600-617.

[10] Zhou L., Li M., Meng G., Zhao H., 2018, An effective cell-based smoothed finite element model for the transient responses of magneto-electro-elastic structures, *Journal of Intelligent Material Systems and Structures* **29**: 3006-3022.

[11] Shooshtari A., Razavi S., 2017, Vibration of a multiphase magneto-electro-elastic simply supported rectangular plate subjected to harmonic forces, *Journal of Intelligent Material Systems and Structures* **28**: 451-467.
[12] Zhang X.L., Chen X.C., Yang E., Li H.F., Liu J.B., Li Y.H., 2019, Closed-form solutions for vibrations of a magneto-electro-elastic beam with variable cross section by means of Green's functions, *Journal of Intelligent Material Systems and Structures* **30**: 82-99.
[13] Mohammadimehr M., Okhravi S.V., Akhavan Alavi S.M., 2018, Free vibration analysis of magneto-electro-elastic cylindrical composite panel reinforced by various distributions of CNTs with considering open and closed circuits boundary conditions based on FSDT, *Journal of Vibration and Control* **24**: 1551-1569.
[14] Kiani A., Sheikhkhoshkar M., Jamalpoor A., Khanzadi M., 2018, Free vibration problem of embedded magneto-electro-thermo-elastic nanoplate made of functionally graded materials via nonlocal third-order shear deformation theory, *Journal of Intelligent Material Systems and Structures* **29**: 741-763.
[15] Farajpour M.R., Shahidi A.R., Hadi A., Farajpour A., 2018, Influence of initial edge displacement on the nonlinear vibration, electrical and magnetic instabilities of magneto-electro-elastic nanofilms, *Mechanics of Advanced Materials and Structures* **26**: 1469-1481.
[16] Vinyas M., 2019, A higher-order free vibration analysis of carbon nanotube-reinforced magneto-electro-elastic plates using finite element methods, *Composites Part B: Engineering* **158**: 286-301.
[17] Xue C.X., Pan E., Zhang S.Y., Chu H.J., 2011, Large deflection of a rectangular magnetoelectroelastic thin plate, *Mechanics Research Communications* **38**: 518-523.
[18] Razavi S., Shooshtari A., 2015, Nonlinear free vibration of magneto-electro-elastic rectangular plates, *Composite Structures* **119**: 377-384.
[19] Shooshtari A., Razavi S., 2015, Linear and nonlinear free vibration of a multilayered magneto-electro-elastic doubly-curved shell on elastic foundation, *Composites Part B: Engineering* **78**: 95-108.
[20] Shabanpour S., Razavi S., Shooshtari A., 2019, Nonlinear vibration analysis of laminated magneto-electro-elastic rectangular plate based on third-order shear deformation theory, Iranian Journal of Science and Technology, *Transactions of Mechanical Engineering* **43**: 211-223.
[21] Ansari R., Gholami R., Rouhi H., 2019, Geometrically nonlinear free vibration analysis of shear deformable magneto-electro-elastic plates considering thermal effects based on a novel variational approach, *Thin-Walled Structures* **135**: 12-20.
[22] Carrera E., Zappino E., 2013, Aeroelastic analysis of pinched panels in supersonic flow changing with altitude, *Journal of Spacecraft and Rockets* **51**: 187-199.
[23] Zhao M.H., Zhang W., 2014, Nonlinear dynamics of composite laminated cantilever rectangular plate subject to third-order piston aerodynamics, *Acta Mechanica* **225**: 1985-2004.
[24] Meijer M.C., Dala L., 2015, Zeroth-order flutter prediction for cantilevered plates in supersonic flow, *Journal of Fluids and Structures* **57**: 196-205.
[25] Chen T., Xu M., Xie D., An X., 2017, Post-flutter response of a flexible cantilever plate in low subsonic flows, *International Journal of Non-Linear Mechanics* **91**: 113-127.
[26] Eugeni M., Mastroddi F., Dowell E.H., 2017, Normal form analysis of a forced aeroelastic plate, *Journal of Sound and Vibration* **390**: 141-163.
[27] Pacheco D.R.Q., Marques F.D., Ferreira A.J.M., 2018, Finite element analysis of fluttering plates reinforced by flexible beams: An energy-based approach, *Journal of Sound and Vibration* **435**: 135-148.
[28] Raja S., Pashilkar A.A., Sreedeep R., Kamesh J.V., 2006, Flutter control of a composite plate with piezoelectric multilayered actuators, *Aerospace Science and Technology* **10**: 435-441.
[29] Song Z.G., Li F.M., 2012, Active aeroelastic flutter analysis and vibration control of supersonic composite laminated plate, *Composite Structures* **94**: 702-713.
[30] Makihara K., Shimose S., 2012, Supersonic flutter utilization for effective energy-harvesting based on piezoelectric switching control, *Smart Materials Research* **2012**: 181645.
[31] Leão L.S., de Lima A.M.G., Donadon M.V., Cunha-Filho A.G., 2016, Dynamic and aeroelastic behavior of composite plates with multimode resonant shunted piezoceramics in series, *Composite Structures* **153**: 815-824.
[32] Lu S.F., Zhang W., Song X.J., 2018, Time-varying nonlinear dynamics of a deploying piezoelectric laminated composite plate under aerodynamic force, *Acta Mechanica Sinica* **34**: 303-314.
[33] Serry M., Tuffaha A., 2018, Static stability analysis of a thin plate with a fixed trailing edge in axial subsonic flow: Possio integral equation approach, *Applied Mathematical Modelling* **63**: 644-659.
[34] Song Z.G., Yang T.Z., Li F.M., Carrera E., Hagedorn P., 2018, A method of panel flutter suppression and elimination for aeroelastic structures in supersonic airflow, *Journal of Vibration and Acoustics* **140**: 064501.
[35] Kelkar A., Deshpande P., Vogel J., 2016, Energy recovery concepts in actively controlled lco instabilities caused by free-play induced aeroelastic flutter, *Proceedings of the First International Symposium on Flutter and its Application*.
[36] de Sousa V.C., Silva T.M.P., Junior C.D.M., 2017, Aeroelastic flutter enhancement by exploiting the combined use of shape memory alloys and nonlinear piezoelectric circuits, *Journal of Sound and Vibration* **407**: 46-62.
[37] de Sousa V.C., Junior C.D.M., Elahinia M.H., 2018, Effect of constitutive model parameters on the aeroelastic behavior of an airfoil with shape memory alloy springs, *Journal of Vibration and Control* **24**: 1065-1085.
[38] de Sousa V.C., Junior C.D.M., Elahinia M., 2017, Aeroelastic behavior of a typical section with shape memory alloy springs: Modeling nonhomogeneous distribution of state variables, *Applied Mathematical Modelling* **52**: 404-416.

[39] Rafiee M., Mohammadi M., Sobhani Aragh B., Yaghoobi H., 2013, Nonlinear free and forced thermo-electro-aero-elastic vibration and dynamic response of piezoelectric functionally graded laminated composite shells, Part I: Theory and analytical solutions, *Composite Structures* **103**: 179-187.

[40] Rafiee M., Mohammadi M., Sobhani Aragh B., Yaghoobi H., 2013, Nonlinear free and forced thermo-electro-aero-elastic vibration and dynamic response of piezoelectric functionally graded laminated composite shells Part II: Numerical results, *Composite Structures* **103**: 188-196.

[41] Arefi M., Ashraf M. Zenkour., 2017, Nonlocal electro-thermo-mechanical analysis of a sandwich nanoplate containing a Kelvin–Voigt viscoelastic nanoplate and two piezoelectric layers, *Acta Mechanica* **228**: 475-493.

[42] Arefi M., Ashraf M. Zenkour., 2017, Thermo-electro-mechanical bending behavior of sandwich nanoplate integrated with piezoelectric face-sheets based on trigonometric plate theory, *Composite Structures* **162**: 108-122.

[43] Ashraf M. Zenkour., Arefi M., 2017, Nonlocal transient electrothermomechanical vibration and bending analysis of a functionally graded piezoelectric single-layered nanosheet rest on visco-Pasternak foundation, *Journal of Thermal Stresses* **40**: 167-184.

[44] Arefi M., Ashraf M. Zenkour., 2019, Effect of thermo-magneto-electro-mechanical fields on the bending behaviors of a three-layered nanoplate based on sinusoidal shear-deformation plate theory, *Journal of Sandwich Structures & Materials* **21**: 639-669.

[45] Arefi M., Ashraf M. Zenkour., 2016, Employing sinusoidal shear deformation plate theory for transient analysis of three layers sandwich nanoplate integrated with piezo-magnetic face-sheets, *Smart Materials and Structures* **25**: 115040.

[46] Arefi M., Zamani M.H., Kiani M., 2018, Size-dependent free vibration analysis of three-layered exponentially graded nanoplate with piezomagnetic face-sheets resting on Pasternak's foundation, *Journal of Intelligent Material Systems and Structures* **29**: 774-786.

[47] Arefi M., Soltan Arani A.H., 2018, Higher order shear deformation bending results of a magnetoelectrothermoelastic functionally graded nanobeam in thermal, mechanical, electrical, and magnetic environments, *Mechanics Based Design of Structures and Machines* **46**: 669-692.

[48] Reddy J.N., 2004, *Mechanics of Laminated Composite Plates and Shells: Theory and Analysis*, Boca Raton, CRC Press.

[49] Li Y.S., Cai Z.Y., Shi S.Y., 2014, Buckling and free vibration of magnetoelectroelastic nano plate based on nonlocal theory, *Composite Structures* **111**: 552-529.

[50] Chia C.Y., 1980, *Nonlinear Analysis of Plates*, McGraw-Hill.

[51] Shiau L.C., Lu L.T., 1992, Nonlinear flutter of two-dimensional simply supported symmetric composite laminated plates, *Journal of Aircraft* **29**: 140-145.

[52] Nayfeh A.H., Dean TMook., *1995, Nonlinear Oscillation*, John Wiley & Sons.

[53] Shooshtari A., Razavi S., 2014, Nonlinear free and forced vibrations of anti-symmetric angle-ply hybrid laminated rectangular plates, *Journal of Composite Materials* **48**: 1091-1111.

[54] Ramirez F., Heyliger P.R., Pan E., 2006, Free vibration response of two-dimensional magneto-electro-elastic laminated plates, *Journal of Sound and Vibration* **292**: 626-644.

[55] Young W.C., Budynas R.G., 2001, *Roark's Formulas for Stress and Strain*, McGraw-Hill.

[56] Ansari R., Gholami R., 2016, Nonlocal free vibration in the pre- and post-buckled states of magneto-electro-thermo elastic rectangular Nano plates with various edge conditions, *Smart Materials and Structures* **25**: 095033-095050.